Antiphase chaos and intensity dependent dissipations

David H. Henderson and Gian-Luca Oppo*
Department of Physics and Applied Physics, University of Strathclyde, 107 Rottenrow, Glasgow G4 0NG Scotland, United Kingdom
(Received 2 September 1998; revised manuscript received 28 October 1998)

The dynamics of a laser with an intracavity second harmonic crystal is analyzed in a model with two modes of one polarization and a third mode orthogonally polarized. In regimes of global mode coupling, antiphase chaos affects all modes while the intensity maxima of the third mode appear locked on a period-one dynamics. We explain this curious feature in terms of periodic decoupling of the modes with orthogonal polarizations and intensity dependent dissipations which force the trajectories onto extremely narrow manifolds. The effect of intensity dependent dissipations on Lyapunov numbers calculated in specific parts of the chaotic attractor is also described. [S1063-651X(99)09402-7]

PACS number(s): 05.45.−a, 42.65.Sf

I. INTRODUCTION

In recent years much attention has focused upon the occurrence of antiphase dynamics in globally coupled multimode lasers. The root of such interest is the pioneering work of Baer [1] on the dynamics generated by a multimode (N coupled modes) solid state laser with losses due to intracavity second harmonic generation. The model introduced by Baer has since been extended significantly by Roy and collaborators [2] to include the effects of the birefringence of the intracavity elements and the polarization of each mode. This model has been studied intensively from a nonlinear dynamics viewpoint both theoretically and numerically. The diverse range of dynamical phenomena encountered include, among others, intermittency [3] and period doubling [4] routes to chaos, elimination of chaos [5], chaotic itinerancy [6] and, more importantly for our analysis, antiphase dynamics [7]. Also, in some instances, good qualitative agreement has been shown between the model and experiments [7,8].

Of particular interest is the occurrence of antiphase dynamics. Here the pulsations of modes with a given polarization are synchronized to that of orthogonally polarized modes. The case of three mode antiphase dynamics is particularly striking and has been studied in some detail in Ref. [9]. Here two modes oscillate orthogonally to a third. The onset of pulsations from the steady state occurs via a Hopf bifurcation [4]. One critical parameter in this system is a geometrical factor g that accounts for the relative angle between the fast axes of the intracavity elements and also phase delays due to the birefringence of such elements. Indeed as g is changed the system is seen to pass through a region of chaotic dynamics after a period doubling cascade. One intriguing finding of Ref. [9] was that while chaos is seen to develop in the dynamics of the two modes of the same polarization, no chaotic behavior appeared in the third orthogonally polarized mode. In their paper, Mandel and Wang described this effect as an effective dynamical independence of the modes due to the antiphase relationship between modes of orthogonal polarizations [9]: ''effective'' in the sense that the modes pulsing with an antiphase relationship are not decoupled in a strict sense. The third mode is then unable to ''see'' the chaotic pulsing of the first two modes and thus remains periodic.

In this paper we show that if one expands the scale of the dynamics of the third mode via a logarithmic transformation of the intensities then chaos is indeed observed in the time evolution of the orthogonally polarized mode because of the coupling among all modes. What remains surprising is the observation that even if the dynamics of the third mode is chaotic, its peak intensity and period remain very close to periodic oscillations. Our main result is to explain this peculiar feature by showing that periodically the third mode becomes decoupled and experiences large intensity dependent dissipations. This forces the trajectory onto a very narrow manifold where widely different initial conditions keep generating very close values of the third mode peak intensity. The intensity maxima of the third mode look periodic but its dynamics is chaotic. We support our explanation with the numerical evaluation of the divergence of the total flow, the divergence of the three modes taken separately and via local Lyapunov numbers.

The paper is organized as follows. The model of Ref. [2] is briefly revised in Sec. II. Here we introduce the logarithmic transformation used to show that chaos affects the dynamics of all three coupled modes (Sec. III). In Sec. III we also show that antiphase dynamics leads to periodic decoupling of the modes. When the third mode has a high intensity, its evolution can be described as an overdamped oscillation in a modified Toda potential. Sec. IV is dedicated to the analysis of the chaotic dynamics in terms of the divergence of the flow. We first show that the time-dependent divergence of the flow greatly simplifies after the logarithmic transformation. We then provide a clear-cut explanation of the ''periodicity'' of the peak intensities of the third mode in terms of periodic dynamical decoupling and intensity dependent dissipations. Sec. V is devoted to another general feature of systems with intensity dependent dissipations: wide variations of Lyapunov numbers in different parts of the phase space. In particular, we show that the maximum (positive) Lyapunov number of antiphase chaos is locally negative when the intensity of the third mode is high. A final discussion and conclusions are contained in Sec. VI.

*Electronic address: gianluca@phys.strath.ac.uk

 ©1999 The American Physical Society

II. THE MODEL

The rate equations for a multimode Nd:YAG ring laser with coupling and losses due to intracavity second harmonic generation of a potassium titanyl phosphate (KTP) crystal are written as [2]

$$\frac{dI_k}{dT}=\left(G_k-\alpha-g\epsilon I_k-2\epsilon\sum_{j\neq k}\mu_{jk}I_j\right)I_k, \tag{1}$$

$$\frac{dG_k}{dT}=\tau\left[\gamma-\left(1+I_k+\beta\sum_{j\neq k}I_j\right)G_k\right], \tag{2}$$

where $k=1,2,\ldots,N$ is the modal index and N the number of modes. Here, I_k and G_k are, respectively, the intensity and gain associated with the kth longitudinal mode; α is the cavity loss parameter, γ is the small-signal gain, and ϵ is a coefficient that gives a measure of the conversion efficiency of the intensity at the fundamental frequency into a mode at the doubled frequency (its value is dependent on the properties of the KTP crystal). Furthermore, $\beta\,(0<\beta<2)$ is a cross saturation parameter that gives a measure of the competition among the various longitudinal modes for a given population inversion, τ is equal to τ_c/τ_f where τ_c is the cavity round-trip time, τ_f is the population lifetime and $T=t/\tau_c$. In this study the ''active'' parameter is g $(0\leqslant g\leqslant 1)$, which corresponds to a geometrical factor dependent upon the orientation of the fast axis of the YAG crystal relative to the fast axis of the KTP crystal and also accounts for the phase delays imposed by these two birefringent intracavity elements. In this system the existence of longitudinal modes of orthogonal polarizations is accounted for by the factor μ_{jk}. As such $\mu_{jk}=g$ if modes j and k have the same polarization and $\mu_{jk}=1-g$ if modes j and k are orthogonally polarized. As in many studies of this system we have made the assumption that α, γ, β, and ϵ are the same for all modes. It is important to note that cross saturation of the active medium $(\beta I_j G_k)$ and sum-frequency generation due to the KTP crystal $(2\epsilon\mu_{jk}I_jI_k)$ ensure global coupling among the modes.

As the small signal gain is increased the solutions of Eqs. (1) and (2) change from the steady state to a periodic oscillation via a Hopf bifurcation [4]. The simplest manifestation of antiphase dynamics is a periodic state in which the modal intensities have similar profiles, but are shifted in time by P/N where P is the period and N is the number of modes. Many different types of dynamical behavior are possible in this system but we will concentrate on the antiphase chaotic regime. Erneux and Mandel [10] have shown that antiphase dynamics can be obtained with as few coupled modes as two. In this paper, however, we want to focus on the possibility of chaotic motion confined to modes with the same polarization during antiphase dynamics. In order to study such a situation the minimum number of coupled modes is $N=3$, modes 1 and 2 having the same polarization and mode 3 being orthogonally polarized.

Mandel and Wang [9] studied the dynamical behavior of the $N=3$-mode case in detail. In particular they showed that for $\tau_c/\tau_f=0.002$, $\beta=0.292$, $\alpha=0.02$, $\gamma=0.095$, $\epsilon=0.05$, and g decreasing from 0.56 to 0.5161 a full period doubling cascade to chaos takes place. The surprising thing is that while the intensities of the first two modes and the total intensity clearly display the doubling and chaotic behavior, the intensity of the third mode appears to remain anchored to a period one oscillation (''dynamical independence''). This intriguing phenomenon appears to be also in agreement with experiments on a Nd:YAG laser with modulated pump [11]. The reasonable explanation provided in Ref. [9] from the direct observation of the intensity pulses is that the antiphase oscillations result in mode 3 evolving with a different dynamics to modes 1 and 2 because ''mode 3 is already off when modes 1 and 2 reach their peaks, and therefore mode 3 does not record the chaotic nature of the other two modes'' [9].

To further investigate the phenomenon of dynamical independence we note that the equations for the intensities I_k contain a multiplicative I_k factor to all terms. This suggests that the dynamics is better unfolded when using a new set of variables $S_k=\ln I_k$ as demonstrated by Oppo and Politi [12] for single-mode lasers of class *B*. After this change of variables, the initial system of equations becomes

$$\dot{S}_k=G_k-\alpha-g\epsilon\exp(S_k)-2\epsilon\sum_{j\neq k}\mu_{jk}\exp(S_j), \tag{3}$$

$$\dot{G}_k=\tau\left[\gamma-\left(1+\exp(S_k)+\beta\sum_{j\neq k}\exp(S_j)\right)G_k\right]. \tag{4}$$

For $\epsilon=\beta=0$ (i.e., no intracavity KTP crystal) one trivially obtains uncoupled rate equations, one set for each longitudinal mode. Such equations correspond to damped oscillations in a Toda potential [12]. A single oscillation in a Toda potential can be separated into a lethargy time T_1 during which the population G_k grows and the output intensity is close to zero and a spike time T_2 during which the peak intensity of the output pulse is reached [12]. It is easy to see that the energy dissipations of a single-mode laser take place mainly during the spike time T_2. In fact, by evaluating the divergence of the flow one obtains

$$\operatorname{div}\mathrm{F}_k=\frac{\partial\dot{S}_k}{\partial S_k}+\frac{\partial\dot{G}_k}{\partial G_k}=-\tau[1+\exp(S_k)]=-\tau(1+I_k), \tag{5}$$

which shows a constant rate of dissipations during the lethargy time and a variable (and, in principle, much larger) rate of dissipations during the spike time. The single-mode laser equations in the logarithmic scaling are perhaps the simplest example of a dynamical system with intensity dependent divergence (i.e., dissipations) in nonlinear optics. Dynamical flows $\mathrm{F}(\mathbf{x})$ with variable dependent dissipations are defined by the condition

$$\operatorname{div}\mathrm{F}(\mathbf{x})=-\boldsymbol{\Gamma}-\mathbf{H}(\mathbf{x}), \tag{6}$$

where Γ is a real number larger or equal to zero and H is a positive definite function of the dynamical variables $\mathbf{x}$. We will see in Sec. IV that Eqs. (3) and (4) form a dynamical flow with intensity dependent dissipations and that this is the reason why the third mode can maintain ''period-one'' peak intensities while modes 1 and 2 display chaotic oscillations.

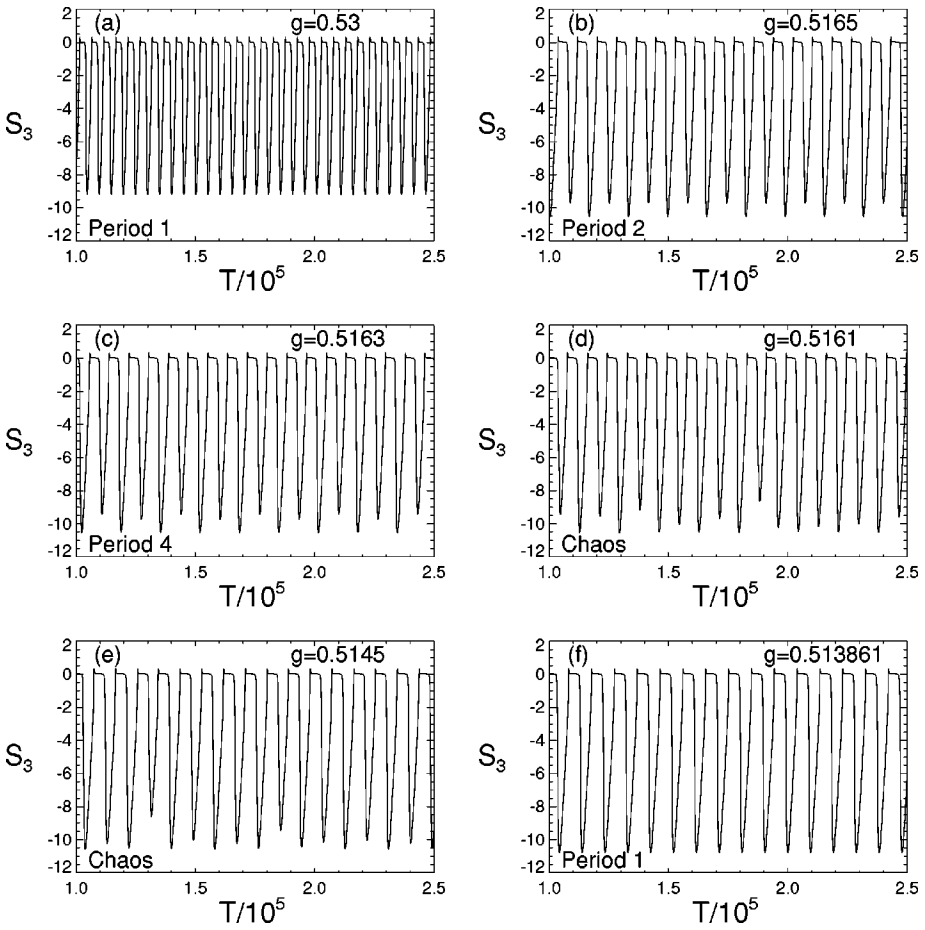

FIG. 1. Period doubling route to chaos in the logarithm (S_3) of the third laser mode intensity. After a chaotic window the system once again returns to periodic behavior displayed in the last panel for $g=0.513\,861$. The other parameters are given at the beginning of Sec. III.

III. ANTIPHASE CHAOS AND PERIODIC DECOUPLING

Our study starts from the numerical investigation of Ref. [9]. We take $\tau_c/\tau_f=0.002$, $\beta=0.292$, $\alpha=0.02$, $\gamma=0.095$, $\epsilon=0.05$ and consider $0.5\leqslant g\leqslant 0.56$. Throughout our numerical analysis we use a standard variable step Adams integrator. We start first from the period doubling cascade leading to chaos for decreasing g from 0.56 to 0.5. It is clear from Figs. 1(a)–1(f), which display the temporal evolution of $S_3=\ln I_3$, that mode 3 follows the same period doubling route to chaos displayed by modes 1 and 2. (Note that all quantities are given in dimensionless units.) One clearly observes oscillating ''minima'' during the lethargy times of mode 3 while the maxima of both I_3 and S_3 would appear to repeat themselves after each period of the fundamental.

Figures 2 and 3 present the main finding of Ref. [9] in the chaotic regime but with $g=0.5145$. The time evolution of the intensity of mode 3 looks periodic while the intensities of the equally polarized modes 1 and 2 display the underlying chaotic dynamics [Figs. 2(b) and 2(c)]. Pulses of modes 1 and 2 still occur at regular intervals since antiphase chaos affects the pulse amplitudes but not their phases [9]. Figure 3(a) shows a three-dimensional projection of the six-dimensional chaotic attractor on the (I_3,G_3,G_1) subspace. The related two-dimensional (2D) projections are presented in Fig. 3(b). For completeness we also present in Fig. 3(c) the projections of the attractor in the (I_1,I_2,I_3) subspace. It is striking to note that while the majority of the 2D projections contain clear signatures of chaos, the 2D projection I_3 vs G_3 looks like a period-one orbit. This phenomenon was interpreted by Mandel and Wang as an effective dynamical independence of orthogonal laser modes where the chaotic dynamics of modes 1 and 2 is not ''recorded'' by mode 3 [9].

The logarithmic transformation helps us to better understand the mode evolution during antiphase dynamics. When the chaotic attractor is unfolded in the (S_3,G_3,G_1) subspace one can see the spreading of the trajectories on all projections (see Fig. 4). In particular, we reproduce the projection (S_3,G_3) of the third orthogonally polarized mode in Fig. 5 where a magnification of the region of the attractor corresponding to large values of the intensity I_3 is also displayed. The chaotic evolution of modes 1 and 2 is indeed recorded by mode 3 since the parameter values correspond to global coupling. What is still intriguing is that the chaos of mode 3 becomes undetectable when monitoring, for example, the maxima of the intensity I_3. This phenomenon cannot be explained by dynamical independence any longer since the logarithmic transformation clearly shows that mode 3 is taking an active part in the antiphase chaos. We note however that during antiphase dynamics mode coupling terms can widely change in magnitude leading to alternance between strong and weak mode-coupling regimes. In particular, whenever I_3 is large while I_1 and I_2 are small, the dynamic evolution of mode 3 is effectively decoupled from modes 1

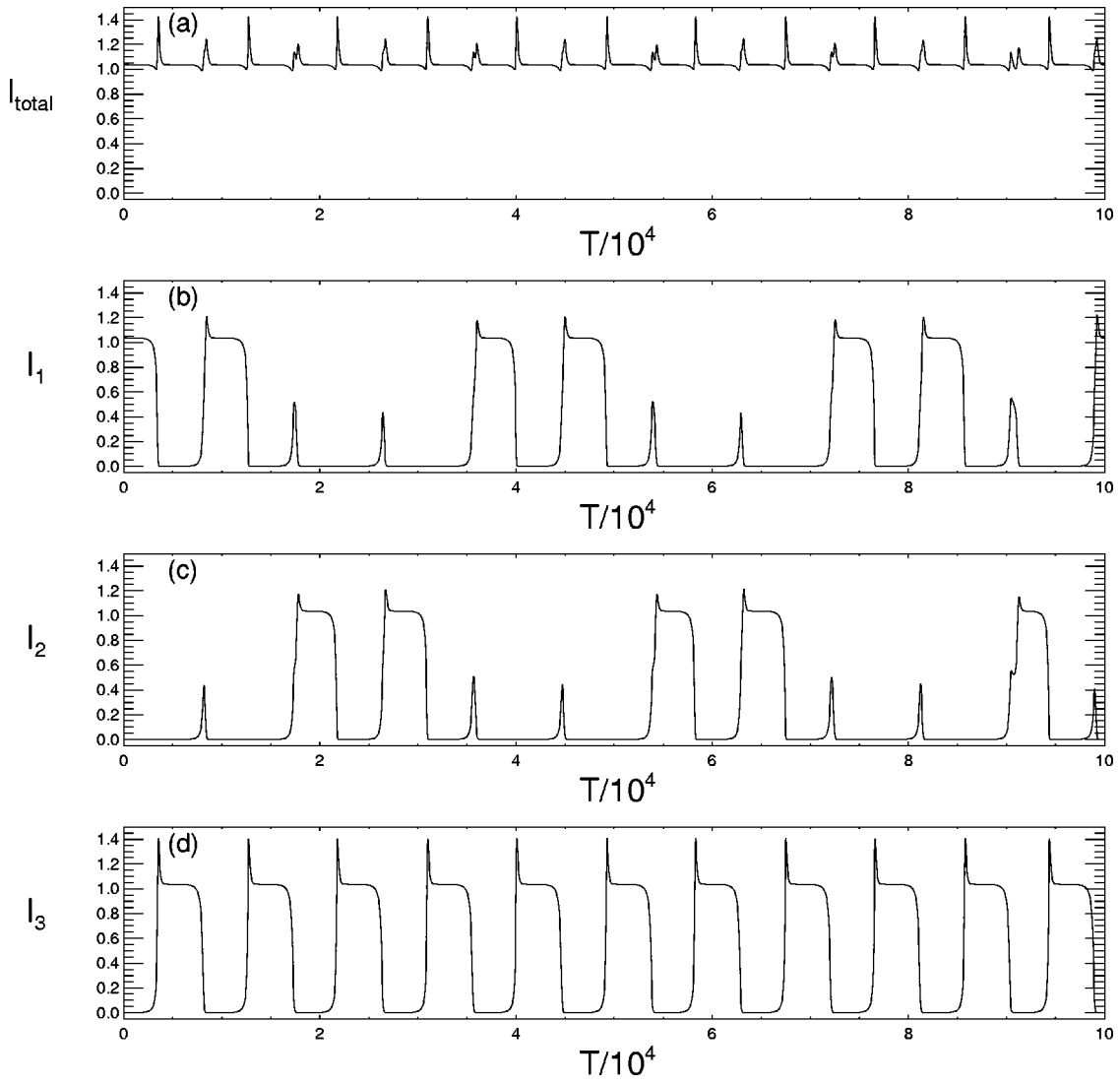

FIG. 2. Time evolution of antiphase chaos in the total intensity I_{tot} (a) and in the modal intensities I_1 (b), I_2 (c), and I_3 (d) for $g=0.5145$. The other parameters are the same as Fig. 1.

and 2 and ruled, to first approximation, by

$$\dot{S}_3 = G_3 - \alpha - g\epsilon \exp(S_3), \tag{7}$$

$$\dot{G}_3 = \tau\{\gamma - [1+\exp(S_3)]G_3\}. \tag{8}$$

This does not mean that mode 3 is decoupled from modes 1 and 2 since their dynamics is strongly affected by the evolution of mode 3. Conversely when I_3 is close to zero, the evolution of modes 1 and 2 affect mode 3 but not vice versa. For brevity we call these dynamical regimes ''decoupled'' and refer to the oscillation between them as ''periodic decoupling.'' However, it is important to note that the decoupling is only unidirectional.

Going back to the situation of $I_3 \gg I_1, I_2$, we obtain from Eqs. (7) and (8) that the temporal evolution of mode 3 is periodically described by the following second-order differential equation

$$\ddot{S}_3 + \tau\dot{S}_3[1+(1+g\epsilon/\tau)\exp(S_3)] + \tau[\alpha-\gamma + (\alpha+g\epsilon)\exp(S_3) + g\epsilon\exp(2S_3)] = 0. \tag{9}$$

Mode 3's dynamics then corresponds to strongly damped oscillations on a time scale of $\sqrt{\tau}$ in a modified Toda potential of the form

$$V(S) = (\alpha+g\epsilon)\exp(S) + \frac{g\epsilon}{2}\exp(2S) - (\gamma-\alpha)S, \tag{10}$$

which is displayed in Fig. 6, with and without the modification $(g\epsilon/2)\exp(2S)$. Damping takes the third mode intensity quickly to the minimum of the potential given by

$$I_{min} = \frac{1}{2}\sqrt{\left(\frac{\alpha}{g\epsilon}-1\right)^2 + \frac{4\gamma}{g\epsilon}} - \frac{1}{2}\left(\frac{\alpha}{g\epsilon}+1\right). \tag{11}$$

The trajectory then remains very close to such a value of I_3 (for the parameters of Fig. 6 $I_{min}=1.036\ldots$) until the coupling with modes 1 and 2 starts to grow. The first effect of the growing intensities I_1 and I_2 is to increase the magnitude of the fixed term α in Eq. (7) thus decreasing the slope of the negative side of $V(S)$ until the minimum I_{min} disappears. Then, the mode-3 intensity begins to drop towards zero. Af-

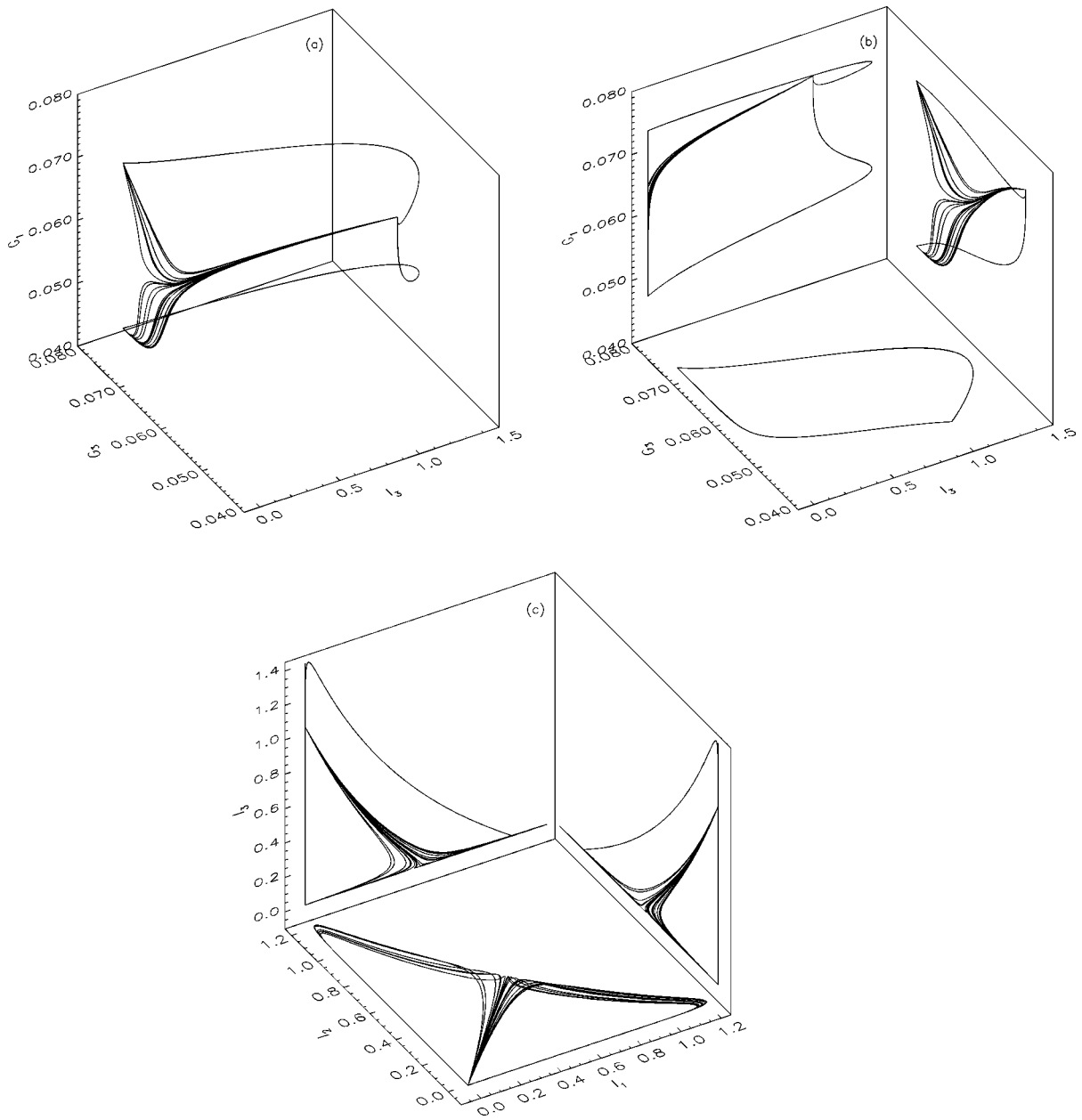

FIG. 3. Projections of the six-dimensional strange attractor during antiphase chaos (a) on the subspace (I_3,G_3,G_1), (b) on the planes (I_3,G_3), (I_3,G_1), and (G_1,G_3), (c) on the planes (I_3,I_2), (I_3,I_1), and (I_2,I_1). The parameters are the same as for Fig. 2.

ter the pulse formed by modes 1 and 2, S_3 is reinjected into the modified Toda potential (10) and the cycle repeats again.

At this stage we should emphasize the difference between the mode-3 dynamics of equations (3) and (4) and that of the decoupled equations (7) and (8) when I_3 is low. In the case of single-mode class-B dynamics, Eqs. (7) and (8) with no losses, it has been shown that ''firing'' of the laser intensity occurs after a long duration (lethargy time) where the population grows slowly [12] (see the flat lower part of the dashed orbit in Fig. 7). The dynamics are quite different when lethargy times occur during antiphase oscillations in the multimode system (3), (4), see Fig. 2. After the single mode I_3 dynamics in the Toda potential loses stability, i.e., escapes from point B of the solid curve in Fig. 7, the system quickly reaches point A where the gain G_3 is at its maximum but it is not able to trigger the next I_3 pulse as yet. In contrast to the single class B mode laser with no losses, it is the destabilization of the orthogonally polarized modes that trigger the next firing of the I_3 intensity via the sudden decrease of the cross-mode losses [see the last term of Eq. (3)]. To further clarify the role played by the gain G_3 during the lethargy time we have plotted, in Fig. 8, the temporal evolution for the antiphase dynamics of Eqs. (3) and (4) [Fig. 8(a)] and for the case of a single-mode class B laser with no losses [Fig. 8(b)]. The vertical dashed lines correspond to the firing times. During the lethargy times of I_3 the dynamics of the third mode is not decoupled from the other modes and the Toda potential picture described above does not apply.

An analogous, yet very different, dynamics takes place during the decoupling at small I_3 values. In this case the dynamics of modes 1 and 2 is described by coupled oscillators in modified Toda potentials. However, since the aim of the next section is to provide a clear-cut explanation of the pseudo-period-one behavior of the maxima of I_3 in terms

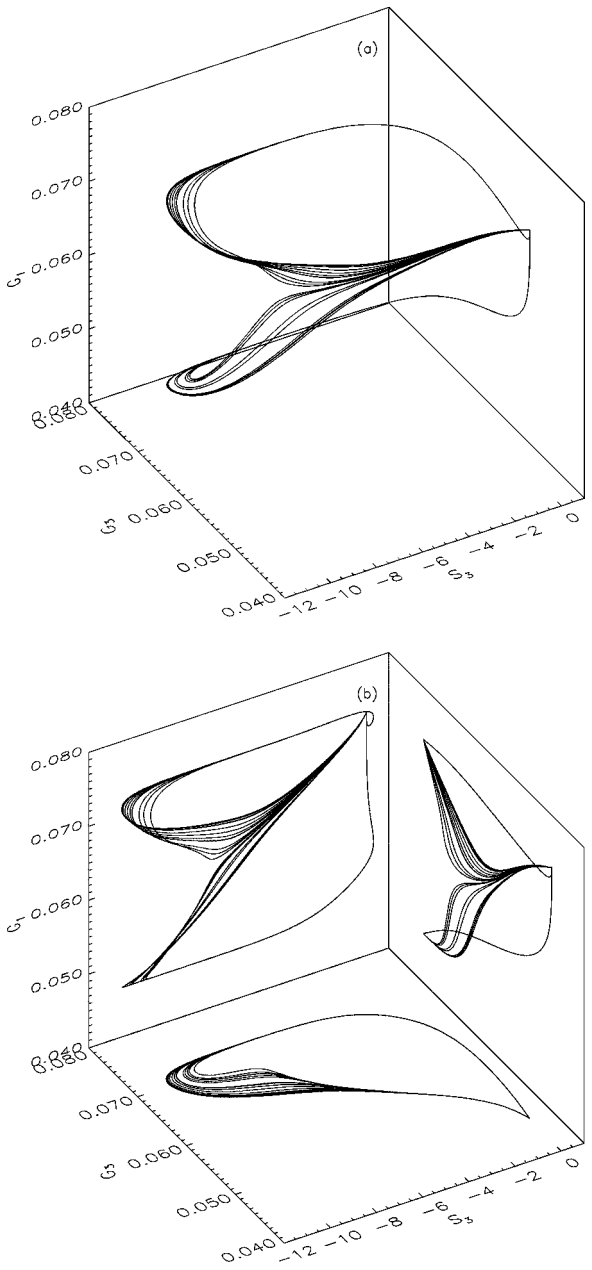

FIG. 4. (a) Projections of the six-dimensional strange attractor during antiphase chaos (a) on the subspace (S_3,G_3,G_1), and (b) on the planes (S_3,G_3), (S_3,G_1), and (G_1,G_3). The parameters are the same as for Fig. 2.

of periodic decoupling and the intensity dependent dissipations we leave this periodically decoupled regime to future studies.

Before concluding this section, we point out that the logarithmic transformation is trivially singular for $I_k=0$ and thus requires initial conditions of all the mode intensities to be as small as desired but different from zero. One may object that the deterministic dynamics may take the trajectory back to $I_k=0$ before the generation of the next k-mode pulse, thus creating problems for the integration of Eqs. (3) and (4). This is, however, not possible since it is easy to show that the surfaces with $I_k=0$ are invariant manifolds of the system and that once $I_k=0$ is reached, then the k mode is removed from the dynamics. To maintain the physical reliability of the model, one needs then to consider the effect of intensity fluctuations when I_k is very small but different from zero. Such fluctuations automatically exclude the possibility of reaching $I_k=0$ and then remove the need of considering the singularity of the logarithmic transformation.

IV. ANTIPHASE CHAOS AND INTENSITY DEPENDENT DISSIPATIONS

The logarithmic transformation introduced in Sec. II not only helps to show that mode 3 is chaotic but also that it can be used to exhibit that the multimode laser model under investigation belongs to the same class of dynamical systems with variable dependent divergence of the kind (5), as the single-mode laser. In the case of a three-mode laser the divergence of the original system (1) and (2) is given by

$$\begin{aligned}\operatorname{div} F_I = {} & G_1+G_2+G_3-3\alpha-2\epsilon[g(I_1+I_2)\\ & +(1-g)(I_1+I_2+2I_3)]-g\epsilon(I_1+I_2+I_3)\\ & -\tau[3+(1+2\beta+g\epsilon/\tau)(I_1+I_2+I_3)].\end{aligned} \tag{12}$$

It is difficult to asses from this form of the divergence, the rate of contraction or expansion of the flow around a generic trajectory. However, after applying the transformation $S_i=\ln I_i (i=1,2,3)$ the divergence of the flow changes to

$$\begin{aligned}\operatorname{div} F_S &= -\tau\{3+(1+2\beta+g\epsilon/\tau)\\ &\quad\times[\exp(S_1)+\exp(S_2)+\exp(S_3)]\}\\ &= -\tau[3+(1+2\beta+g\epsilon/\tau)(I_1+I_2+I_3)]\\ &= -\tau[3+(1+2\beta+g\epsilon/\tau)I_{tot}].\end{aligned} \tag{13}$$

A first inspection shows that the instantaneous value of the divergence at a generic time t differs before and after the logarithmic transformation. Since such a transformation is nonlinear but everywhere invertible (once the invariant manifolds correspondent to $I_k=0$ are removed), the asymptotic time-average value of the divergence defined as

$$\langle \operatorname{div} F\rangle = \lim_{T\to\infty}\frac{1}{T}\int_0^T (\operatorname{div} F)\,dt \tag{14}$$

is invariant under the logarithmic transformation. A simple comparison of Eqs. (12) and (13) implies that the time average of the quantity Θ defined as

$$\begin{aligned}\langle\Theta\rangle \equiv \langle & G_1+G_2+G_3-3\alpha-2\epsilon[g(I_1+I_2)\\ & +(1-g)(I_1+I_2+2I_3)]-g\epsilon(I_1+I_2+I_3)\rangle\end{aligned} \tag{15}$$

tends to zero as $T\to\infty$. This is numerically verified, for example, for the antiphase chaos of Eqs. (1) and (2) in Fig. 9. It is important to note that the time-averaged asymptotic dissipations are independent of the gain variables and of the cavity losses α, a nontrivial result that would not appear unless the logarithm transformation of Ref. [12] is employed.

Thus the logarithmic transformation serves not only to uncover the hidden dynamics of the mode-3 intensity but also to show clearly that the dissipations in this system are intensity dependent. There is nothing strange in the nondissipative nature of the cavity loss terms since part of the en-

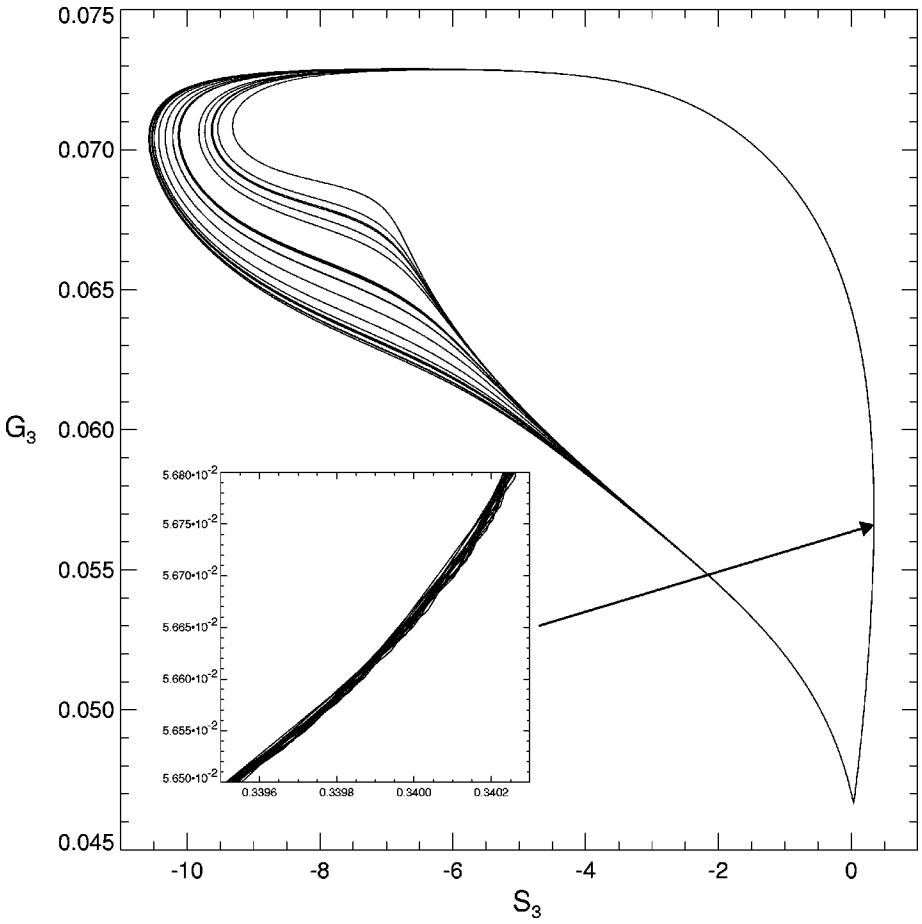

FIG. 5. Projection of the six-dimensional strange attractor during antiphase chaos on the plane (S_3, G_3). The inset shows a region of the attractor with heavy contraction. The parameters are the same as for Fig. 2.

ergy provided by the external pump γ is extracted in the laser output. Thus the terms accounting for the effect of the output mirrors in the original equations describe processes of energy flow and not of energy loss as gorgeously outlined in [12].

Expression (13) unequivocally shows that the model of the three-mode laser with intracavity second harmonic generation belongs to the class of dynamical systems with intensity dependent dissipations. Note also that this result is also valid in the case of a generic number of modes N since the divergence of the transformed flow is

$$\mathrm{div}\, F_S = -\tau\{N + [1 + (N-1)\beta + g\epsilon/\tau] I_{tot}\}. \qquad (16)$$

One of the major implications of Eqs. (13) and (16) is that each orbit of the dynamical system experiences different levels of contraction depending upon the region of phase space it currently resides in. Dissipations increase when the total intensity increases while they remain close to a constant rate if all the mode intensities are low. For the values of the parameters of the antiphase chaos of Figs. 2 and 3, we find that the total intensity contribution to the dissipations $-\tau I_{tot}(1 + 2\beta + g\epsilon/\tau)$ is always between 5 and 7 times larger than the fixed contribution given by -3τ. It is also important to note that more than 95% of the intensity dependent contribution to the dissipations comes from the terms that describe the intensity dependent losses due to second harmonic generation in the Eqs. (1). Finally, the particular form of Eq. (13) allows us to define a contribution to the total dissipation per mode given by

$$\mathrm{div}\, F_k \equiv -\tau\{1 + [1 + (N-1)\beta + g\epsilon/\tau] I_k\}. \qquad (17)$$

It is useful for our purposes to separate the different terms in the single-mode divergence according on their physical origin. The first term $-\tau$ represents losses due to spontaneous emission. The term $-\tau(1 + g\epsilon/\tau) I_k$ is labeled here as ''self''-mode dissipation and is composed of single-mode laser intensity losses [cf. Eq. (5)] and dissipation due to the intensity losses in the second harmonic generation. Finally, the term $-\tau(N-1)\beta I_k$ is labeled here as ''cross''-mode dissipation and describes losses due to mode k on modes $j \neq k$ through the second harmonic intracavity crystal.

We have numerically evaluated the total and single-mode dissipations during antiphase dynamics and, in particular, antiphase chaos. Since the total intensity during antiphase chaos remains always above a certain value (0.98 for the parameter configuration of Fig. 2), the chaotic attractor does not visit regions of the phase space where the total dissipation is low. Things are very different for the dissipations associated with each mode (17) since the modal intensities oscillate from close to zero to just below 1.5 in our normalized units. When I_k is smaller than say 10^{-2} the contribution of mode k to the dissipations is negligible. Then, only the modes with sufficiently large intensity during a cycle of the antiphase dynamics contribute to the energy dissipations. In

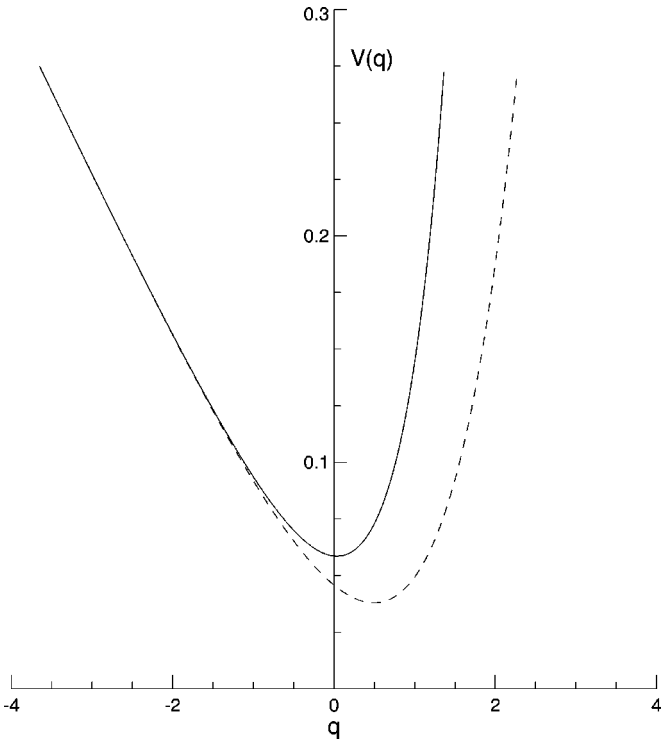

FIG. 6. Modified Toda potential (10) for the same parameters as Fig. 2 (solid line). The dashed curve shows the Toda potential without the modification $g\epsilon/2\ \exp(2S)$ induced by the second harmonic crystal.

particular, we note that during half of the antiphase cycle while I_3 is low, both modes 1 and 2 can provide nonnegligible contributions to the dissipations. However, during the opposite phase of the antiphase cycle, mode 3 takes responsibility for the majority of the system dissipations. Since

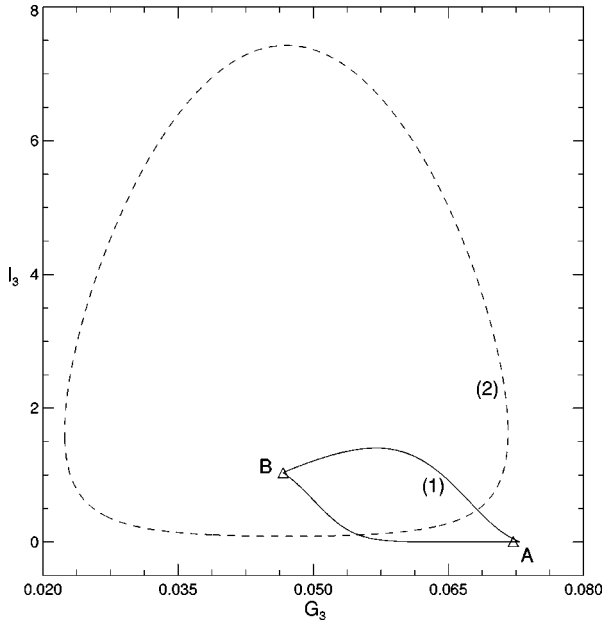

FIG. 7. I_3 vs G_3 oscillations. (1): Motion generated in the multimode system. Points A and B represent quasisteady states of I_3 and G_3. (2): Shifted $(G_3+0.027)$ oscillations in the single-mode laser Toda potential.

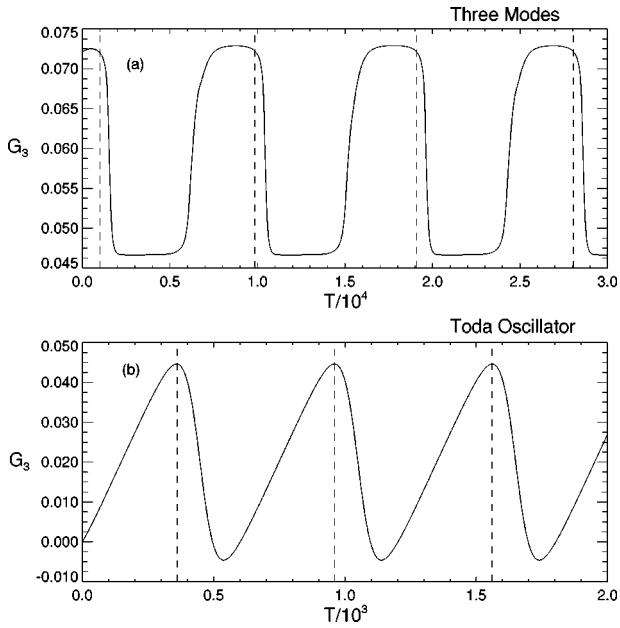

FIG. 8. G_3 vs time in the three-mode laser (a) and the undamped single-mode laser (b). Dashed lines indicate intensity pulse firing.

the total dissipations have a fairly small excursion, we expect from these considerations that, on average, mode 3 contributes almost twice as much to the system divergence as modes 1 and 2 taken individually. This effect is simply a result of the antiphase nature of the oscillations and is clearly verified in Fig. 10 (apart from an obvious bias term $-\tau$ due to the constant contribution from the spontaneous emission of each mode) where the calculation of the asymptotic time-averaged dissipations of the entire flow and that due to all modes taken separately are presented.

Let us focus now on the dissipations during periodic decoupling with large I_3 and small I_1 and I_2. It is easy to see that the total dissipations (16) are mainly given by the spontaneous emission contribution -3τ due to all modes and by

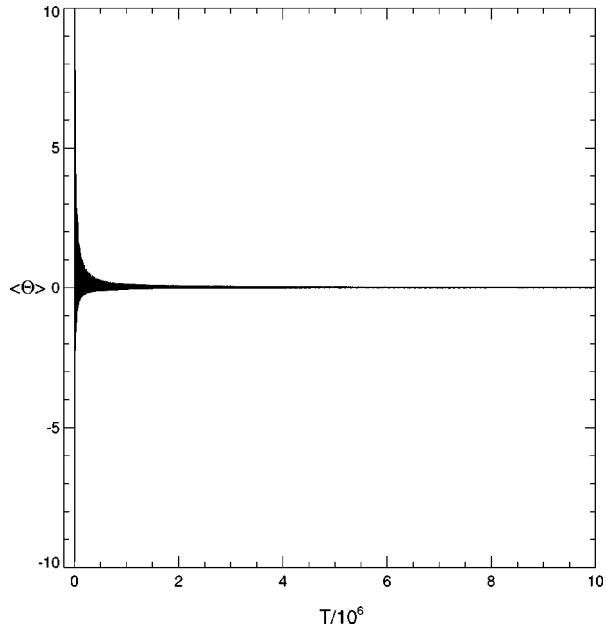

FIG. 9. Time average of the quantity Θ of Eq. (15).

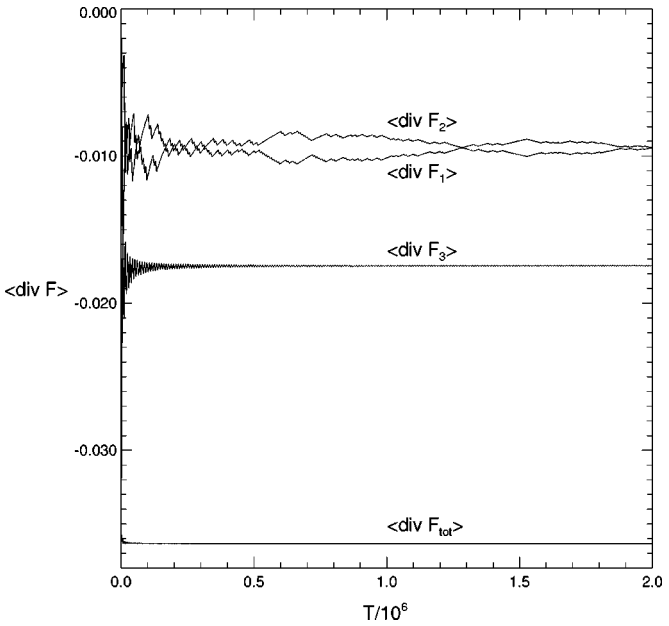

FIG. 10. Plots of the time average of the contribution to the divergence of each mode $\langle \mathrm{div}\, F_i \rangle$ $(i=1,3)$ and the total system divergence $\langle \mathrm{div}\, F_{tot} \rangle$.

an intensity dependent contribution $-(1+2\beta+g\epsilon/\tau)I_3$ due to the third mode only [see Eq. (17)]. Due to periodic decoupling, the dynamics on the two dimensional projection (I_3,G_3) is described by Eq. (9) and the dissipations on such a plane are due to single-mode spontaneous emission and the self-mode terms

$$D_1 \equiv -\tau[1+(1+g\epsilon/\tau)I_3]. \tag{18}$$

This immediately means that the dissipations in the four-dimensional projection space (I_1,G_1,I_2,G_2) are given by

$$D_2 \equiv -2\tau[1+\beta I_3], \tag{19}$$

and are due to spontaneous emission and cross-mode terms. The fact that D_2 contains I_3 is no surprise since (I_1,G_1,I_2,G_2) are affected by the dynamics of the third mode during periodic decoupling and there are cross-mode losses induced by the second harmonic crystal. It is easy to see that the contribution D_1 is far bigger than D_2 and as such it constitutes the largest contribution to the total dissipation whenever I_3 is large. This is numerically verified in Table I where the separate contributions to the dissipations are divided into two categories $(I_3>s$ and $I_3<s)$, averaged in time and tabled for different values of the threshold s during the antiphase chaos. It is then possible to conclude that during periodic decoupling at large intensities of the third mode the largest amount of dissipations take place on the two-dimensional sections, (I_3,G_3) thus squeezing the chaotic manifold to a narrow sheet. Whatever the values of (I_1,G_1,I_2,G_2) provided that I_1 and I_2 are small, the projections of the chaotic trajectories on the (I_3,G_3) section [or equivalently on the (S_3,G_3) sections] will approach each other at an exponential rate of $\delta=-3\times10^{-2}$ (see the first column of Table I). This means that regardless of the injection values of I_3 and G_3 into the modified Toda potential, intensity dependent dissipations will quickly relax their values close to the same trajectory and the chaotic dynamics will keep passing in the vicinity of the same values of I_3 (or S_3) over and over again. This fact combined with the amplitude nature of antiphase chaos [9] forces very similar values of I_3 (or S_3) and G_3 to be repeated after one period of the antiphase dynamics in agreement with what was observed in Figs. 3(b) and Fig. 5 (especially its inset).

TABLE I. Contributions to the divergence D_1 [see Eq. (18)], and D_2 [see Eq. (19)] and total divergence [see Eq. (13)] above and below threshold values s of the intensity I_3. Columns one and two are the divergence contribution D_1, column three is the contribution D_2 while columns four and five contain the data for the total flow divergence.

s	$D_1/10^{-2}$ $(I_3>s)$	$D_1/10^{-2}$ $(I_3<s)$	$D_2/10^{-2}$ $(I_3>s)$	$\mathrm{div}\,F/10^{-2}$ $(I_3>s)$	$\mathrm{div}\,F/10^{-2}$ $(I_3<s)$
0.1	−2.8703	−0.2237	−0.5125	−3.6298	−3.6380
0.2	−2.9521	−0.2239	−0.5159	−3.6316	−3.6356
0.3	−2.9908	−0.2552	−0.5176	−3.6331	−3.6338
0.4	−3.0156	−0.2654	−0.5186	−3.6346	−3.6322
0.5	−3.0341	−0.2799	−0.5194	−3.6360	−3.6308
0.6	−3.0495	−0.2973	−0.5200	−3.6375	−3.6293
0.7	−3.0637	−0.3202	−0.5206	−3.6277	−3.6334
0.8	−3.0778	−0.3546	−0.5212	−3.6258	−3.6334
0.9	−3.0937	−0.4172	−0.5219	−3.6446	−3.6233
1.0	−3.1166	−0.6055	−0.5229	−3.6526	−3.6190

We would like to stress that the explanation of the pseudo-period-one behavior of the dynamics of I_3 provided here is based on two fundamental ingredients: (a) periodic decoupling, which makes the dynamics of I_3 and G_3 negligibly affected by the other variables whenever I_3 is large and I_1 and I_2 are small, and (b) intensity dependent dissipations that explain why the chaotic attractor is squeezed in this part of the phase space to a narrow sheet (see the inset of Fig. 5). It is also relevant to add that the narrowness of the intersection of the chaotic attractor with the (S_3,G_3) plane displayed in Fig. 5 does not mean that the attractor is a tube since orbits that appear very close in Fig. 5 may be quite distant from each other in the complete phase space.

V. GLOBAL AND LOCAL LYAPUNOV EXPONENTS

An objection to the explanation provided in the last section for the appearance of pseudo-period-one behavior of the third mode is that the presence of positive Lyapunov numbers has not been taken into consideration. In this section we focus first on the spectrum of the global Lyapunov numbers during antiphase chaos and show that the magnitude of the largest Lyapunov number cannot affect the strong contraction rates discussed above. More dramatically, we show also that the strong intensity dependent dissipations due to large I_3 can have crucial effects on ''local'' Lyapunov numbers, i.e. contraction (expansion) rates calculated in specific regions of the phase space.

Fig. 11 shows a calculation of the Lyapunov spectrum for the antiphase chaos at $g=0.5145$. Note the very long numerical integration necessary to obtain well defined asymptotic quantities (see inset of Fig. 11). We have checked the correctness of the numerical result by comparing the sum

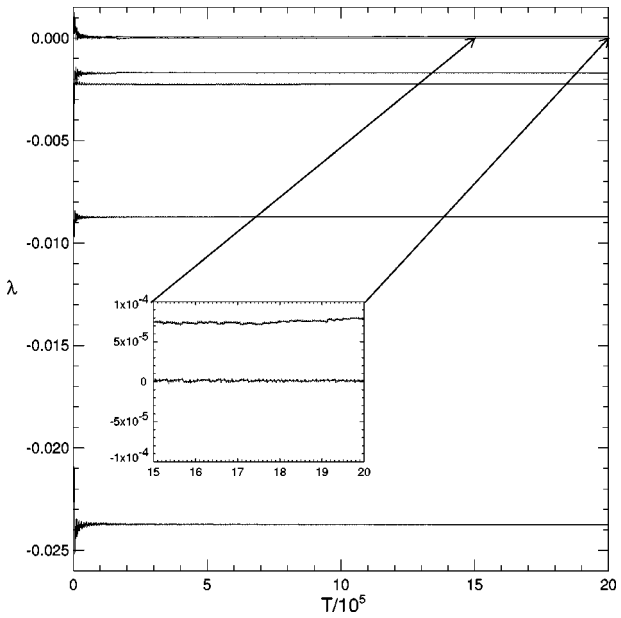

FIG. 11. Asymptotic convergence of the Lyapunov spectrum during antiphase chaos. The parameters are the same as for Fig. 2. The inset shows an expanded view of the two largest Lyapunov exponents.

of all six Lyapunov numbers and the asymptotic total divergence (see Fig. 10). In spite of the very different numerical methods used we obtained $\langle \mathrm{div}\, F\rangle = -3.633\,433\times 10^{-2}$ and $\Sigma_i \lambda_i = -3.633\,526\times 10^{-2}$, i.e., a difference less than 10^{-6}. The slow rate of asymptotic convergence of Lyapunov number calculations (and of the time averaged divergences as shown in the last section) is an intrinsic aspect of systems with variable dependent dissipations since rates of contraction and expansion change in different regions of the phase space. The convergence rate for the evaluation of the maximum Lyapunov number with a given accuracy is in our case up to 100 times longer than, for example, in the Lorenz chaotic attractor, which has a constant dissipation rate over the entire phase space.

The analysis of the Lyapunov spectrum shows that the antiphase chaos described here is fairly weak since there is only one positive eigenvalue two orders of magnitude smaller than the flow divergence. During periodic decoupling at large values of I_3 the rate of contraction on the two-dimensional plane (I_3, G_3) is of the order of $\delta = -3 \times 10^{-2}$, i.e., more than two orders of magnitude bigger than the largest positive Lyapunov number. This clearly proves that the direction of orbit separation, if any, has to be perpendicular to the (I_3, G_3) plane in agreement with our previous picture of the topology of the chaotic attractor as a narrow sheet in this region of the six-dimensional phase space.

The independence of the pseudo-period-one dynamics of mode 3 from the presence of antiphase chaos (i.e., positive Lyapunov numbers) is further justified when we consider the effect of strong intensity dissipations on the largest positive Lyapunov number. We have separated the calculation of the largest Lyapunov number above and below a certain threshold value s of the intensity I_3. These numerical values are defined as ''local'' Lyapunov numbers because they refer only to a part of the strange attractor. The list of local Lyapunov numbers for different values of s in presented in Table II. During periodic decoupling with large I_3 the local Lyapunov number which on average will generate the largest positive Lyapunov number, turns negative. We verify the correctness of these calculations by checking that the sum of the two local Lyapunov numbers (above and below s) keeps generating the largest time-averaged Lyapunov number once the time averages are appropriately taken into account (see the third column of Table II). The fact that the local Lyapunov number is negative has a negligible effect on what was described above. Orbits are getting closer not only in the (I_3, G_3) projections but also in all other projections yet with a much smaller contraction rate. The local Lyapunov number turning negative with large I_3 is also in perfect agreement with the difference in asymptotic total divergences above and below s as shown in last two columns of Table I. Such a difference may appear to be small but is enough to counteract the effect of the small positive Lyapunov number.

TABLE II. Local maximum Lyapunov exponent above and below threshold values s of the intensity I_3. The third column contains the sum of the local Lyapunov contributions suitably averaged in time.

s	$\lambda_{max}/10^{-3}$ $(I_3 > s)$	$\lambda_{max}/10^{-3}$ $(I_3 < s)$	$\lambda_{max}/10^{-3}$
0.1	0.2588	−0.1482	0.07615
0.2	0.1637	−0.02346	0.07615
0.3	0.09017	0.06081	0.07615
0.4	0.03153	0.1236	0.07615
0.5	−0.02019	0.1761	0.07615
0.6	−0.07264	0.2269	0.07615
0.7	−0.1308	0.2803	0.07615
0.8	−0.2005	0.3394	0.07615
0.9	−0.2900	0.4044	0.07615
1.0	−0.4333	0.4589	0.07615

One may object that a similar alternance between local positive and local negative Lyapunov numbers can also take place for the first negative Lyapunov exponent, thus reintroducing the local chaos for large I_3. This, however, cannot be the case since the difference between the asymptotic total divergences above and below s cannot justify an excursion of local Lyapunov numbers of the order of 10^{-3}.

VI. CONCLUSIONS

In this paper we have shown that energy dissipations in models of lasers with intracavity second harmonic generation occur mainly at high output powers via nonlinear losses due to the KTP crystal. Another generic feature of these systems is the occurrence of antiphase dynamics due to competing modes of orthogonal polarizations. The combination of these two generic features results in a splitting of dissipations between the two groups of orthogonally polarized modes. In the case of a group of equally polarized modes being formed by just one laser mode, dissipations are concentrated in the region of the phase space where the intensity of such a lone mode is high and its dynamics are not affected by the other modes (periodic decoupling). In such a region the attractor (chaotic or periodic) is strongly compressed to a very narrow

manifold perpendicular to the plane of the intensity and gain of the lone mode. Such narrowing can be so strong that local Lyapunov numbers (i.e. local rates of convergence or divergence of neighboring orbits) can be seriously affected to the extent that they are all negative even in the presence of chaotic motion. The final and most intriguing effect of the intensity dependent dissipations in systems with antiphase chaotic dynamics is that the maxima of the intensity of the lone mode in one polarization appear periodic in spite of the underlying chaotic motion that affects and couples all of the laser modes.

We have first used a logarithmic transformation of the mode intensities [12] to show that terms usually associated with energy dissipations, such as cavity losses, correspond in real dynamical terms to energy flows. Then, for a three-mode laser with modes 1 and 2 polarized orthogonally to mode 3, we have provided theoretical and numerical evidence of periodic decoupling (where the third mode affects the dynamics of modes 1 and 2 but the inverse is not true), intensity dependent dissipations and strong phase-space contraction when the intensity of mode 3 is large. As a consequence chaotic trajectories are funnelled into a narrow manifold where displacements perpendicular to the trajectory on a (I_3, G_3) projection relax exponentially at a rate of approximately 3×10^{-2} in normalized time units. With a single positive Lyapunov exponent of the order of 10^{-4} the attractor is so strongly squeezed that exponential divergence of nearby trajectories becomes impossible to detect when monitoring large intensities I_3. This corresponds to forcing many different orbits on the same chaotic attractor to generate almost the same value for the peak of the intensity of mode 3 as observed in the numerical simulations. As a consequence, periodic decoupling and intensity dependent dissipations extend and further elucidate the idea of the effective ''dynamical independence'' of orthogonal modes suggested in Ref. [9] as the mechanism for the explanation of period-one-like oscillations of mode-3 intensity during chaotic dynamics of a three-mode laser with intracavity second harmonic generation.

The effects described here are robust deterministic features that are only marginally affected by noise. In fact, antiphase chaos, and consequently periodic decoupling, has already been shown to survive noisy dynamics while it is trivial to show that average contraction rates remain unaltered when small noise terms are added to the dynamical equations. This means that our explanation of the pseudo-period-one behavior of the third orthogonally polarized mode during antiphase chaos, which is based on the intensity dependent dissipations is robust to stochastic perturbations.

Before concluding we would like to stress that the pseudo-period-one oscillation of mode 3 during chaotic evolution is just one of the many phenomena associated with variable dependent flow divergence typical of single and multimode class-*B* lasers. For example, in limiting cases of class-*B* lasers with injected signals [13] or coupled to each other [14], phase-space dependent contraction rates coupled to reversibility leads to coexistence of conservative and dissipative dynamics. Here we have presented evidence that local Lyapunov numbers can be strongly affected by flow divergences which are variable dependent. Such a phenomenon is no surprise if one thinks about the phase space separated in regions of high expansion rates and regions of high contraction rates. The dynamical behavior of the laser output depends on both the local (contraction rates) and global (chaos) topology of the phase space visited by the trajectory.

ACKNOWLEDGMENTS

We thank G. Connolly, S. C. Lyons, and L. S. Phillips for useful discussions. We acknowledge EPSRC (Grant No. GR/L 27916) and the European Commission (TMR Network QSTURCT) for financial support.

[1] T. Baer, J. Opt. Soc. Am. B **3**, 1175 (1986).
[2] R. Roy, C. Bracikowski, and G. E. James, in *Recent Developments in Quantum Optics*, edited by R. Inguva (Plenum Press, New York, 1993), p. 309.
[3] G. E. James, E. M. Harrell II, and R. Roy, Phys. Rev. A **41**, 2778 (1990).
[4] J. Wang and P. Mandel, Phys. Rev. A **48**, 671 (1993).
[5] G. E. James, E. M. Harrell II, C. Bracikowski, K. Wiesenfeld, and R. Roy, Opt. Lett. **15**, 1141 (1990).
[6] K. Otsuka, T. Nakamura, J. Y. Wang, and J. L. Chern, Quantum Semiclassic. Opt. **8**, 1179 (1996).
[7] K. Wiesenfeld, C. Bracikowski, G. E. James, and R. Roy, Phys. Rev. Lett. **65**, 1749 (1990); C. Bracikowski and R. Roy, Chaos **1**, 49 (1991).
[8] D. Y. Tang and N. R. Heckenberg, Phys. Rev. A **56**, 1050 (1997).
[9] P. Mandel and J. Wang, Opt. Lett. **19**, 533 (1994).
[10] T. Erneux and P. Mandel, Phys. Rev. A **52**, 4137 (1995).
[11] N. B. Abraham, L. L. Everett, C. Iwata, and M. B. Janicki, Proc. Soc. SPIE **2095**, 128 (1994).
[12] G.-L. Oppo and A. Politi, Z. Phys. **59**, 111 (1985).
[13] A. Politi, G.-L. Oppo, and R. Badii, Phys. Rev. A **33**, 4055 (1986).
[14] D. H. Henderson and G.-L. Oppo (unpublished).